17, pp. 1020–1040, Nov. 1969.
[8] R. H. Tancrell and M. G. Holland, "Acoustic surface wave filters," *Proc. IEEE*, vol. 59, pp. 393–409, Mar. 1971.
[9] C. Atzeni and L. Masotti, "A new sampling procedure for the synthesis of linear transversal filters," *IEEE Trans. Aerosp. Electron. Syst.*, vol. AES-7, pp. 662–670, July 1971.
[10] H. E. Kallmann, "Transversal filters," *Proc. IRE*, vol. 28, pp. 302–310, July 1940.
[11] R. H. Tancrell *et al.*, "Dispersive delay lines using ultrasonic surface waves," *Proc. IEEE* (Lett.), vol. 57, pp. 1211–1213, June 1969.
[12] R. H. Tancrell and R. C. Williamson, "Wavefront distortion of acoustic surface waves from apodized interdigital transducers," *Appl. Phys. Lett.*, vol. 19, pp. 456–459, Dec. 1971.
[13] R. H. Tancrell, private communication.
[14] E. L. Key, E. N. Fowle, and R. D. Haggarty, "A method of designing signals of large time-bandwidth product," *IRE Int. Conv. Rec.*, pt. 4, pp. 146–155, 1961.
[15] R. M. Artz, E. Saltzmann, and K. Dransfeds, "Elastic surface waves in quartz at 316 MHz," *Appl. Phys. Lett.*, vol. 10, pp. 165–167, Mar. 1967.
[16] G. A. Coquin and H. F. Tiersten, "Analysis of the excitation and detection of piezoelectric surface waves in quartz by means of surface electrodes," *J. Acoust. Soc. Amer.*, vol. 41, pp. 921–939, Apr. 1967.
[17] J. de Klerk and R. M. Daniel, "Investigation to improve microwave acoustic delay lines," Final Rep., Contract F19628-68-C-0236, Mar. 1969.
[18] R. M. White, "Surface elastic waves," *Proc. IEEE*, vol. 58, pp. 1238–1276, Aug. 1970.
[19] H. E. Rowe, *Signals and Noise in Communication Systems*. Princeton, N.J.: Van Nostrand, 1965.
[20] C. C. Tseng, "Frequency response of an interdigital transducer for excitation of surface elastic waves," *IEEE Trans. Electron Devices*, vol. ED-15, pp. 586–594, Aug. 1968.
[21] H. Engan, "Excitation of elastic surface waves by spatial harmonics of interdigital transducers," *IEEE Trans. Electron Devices*, vol. ED-16, pp. 1014–1017, Dec. 1969.
[22] C. C. Tseng and H. Engan, "Comments on 'Excitation of elastic surface waves by spatial harmonics of interdigital transducers,'" *IEEE Trans. Electron Devices* (Lett.), vol. ED-17, pp. 945–946, Oct. 1970.
[23] C. Atzeni, "Sensor number minimization in acoustic surface-wave matched filters," *IEEE Trans. Sonics Ultrason.*, vol. SU-18, pp. 193–201, Oct. 1971.
[24] P. H. Carr, "The generation and propagation of acoustic surface waves at microwaves frequencies," *IEEE Trans. Microwave Theory Tech. (Special Issue on Microwave Acoustics)*, vol. MTT-17, pp. 845–855, Nov. 1969.
[25] C. Atzeni, L. Masotti, and E. Teodori, "Acoustic surface-wave matched filters," *Alta Freq.*, vol. 40, pp. 506–512, June 1971.
[26] J. J. Kroszczyński, "Pulse compression by means of linear period modulation," *Proc. IEEE*, vol. 57, pp. 1260–1266, July 1969.
[27] C. Atzeni and L. Masotti, "Acoustic surface-wave processor for hyperbolic FM signals," *Electron. Lett.*, vol. 7, pp. 693–694, Nov. 1971.
[28] A. Papoulis, *The Fourier Integral and Its Applications*. New York: McGraw-Hill, 1962.
[29] C. Atzeni and L. Masotti, unpublished paper.
[30] R. C. Williamson, "Improved electrostatic probe for measurement of elastic surfaces waves," M.I.T. Lincoln Lab., Cambridge, Mass., Rep., 1971.
[31] R. W. Hamming, *Numerical Methods for Scientists and Engineers*. New York: McGraw-Hill, 1962.
[32] C. Lanczos, *Discourse on Fourier Series*. London, England: Oliver Boyd, 1966.
[33] C. Atzeni and L. Masotti, "Weighted interdigital transducers for smoothing of ripples in acoustic surface wave filters," *Electron. Lett.*, vol. 8, pp. 485–486, Sept. 1972.
[34] G. S. Kino and H. Matthews, "Signal processing in acoustic surface wave devices," *IEEE Spectrum*, vol. 8, pp. 22–35, Aug. 1971.

A Generalized Design Technique for Practical Distributed Reciprocal Ladder Networks

RALPH LEVY

***Abstract*—A generalized design approach is presented for ladder networks consisting of a cascade of constituent two-port networks connected by short lengths of transmission lines. The design is made possible by the derivation of simple equations which define the inverter impedance and associated reference planes of any passive lossless reciprocal two-port. This enables the general ladder network to be equated to a prototype network at a reference frequency. An example is given of the design of a coaxial low-pass filter where fringing capacitances are compensated automatically.**

Introduction

A DISTRIBUTED reciprocal ladder network illustrated in Fig. 1 is defined here as a cascade of reciprocal two-port subnetworks connected by means of transmission lines, which are usually all of approximately equal length and electrically short (between 0 and $3\lambda g/4$). The network is assumed to be lossless. The subnetworks may consist of simple primarily lumped elements such as inductive or capacitive irises or series gaps in a stripline, or distributed elements such as stubs or lengths of transmission line, or may be mixed lumped and distributed in character. Examples of such ladder networks are direct-coupled waveguide bandpass filters, coaxial low-pass filters, impedance transformers, or multielement directional couplers. The latter are four-ports, but if symmetrical, may be decomposed into two-port even- and odd-mode networks, and hence may be included in our category.

A large number of papers have been published on the design of individual ladder-network components, and a few have included a discussion of theoretical design features common to a wider class of structures. Examples of the latter include the use of lumped-element prototypes in the design of direct-coupled filters and the general concept of the impedance inverter by Cohn [1]. Another example is the introduction of the quarter-wave transformer as a prototype circuit for the design of many ladder networks by Young [2].

The result of a typical distributed network synthesis is an idealized component often consisting of a cascade of equal length (commensurate) lines, with or without commensurate stubs. In practice, the component will have junction and dis-

Manuscript received December 6, 1972; revised March 23, 1973.
The author is with Microwave Development Laboratories, Inc., Natick, Mass. 01760.

continuity effects which must be compensated or taken into account if the specification is to be met. For example, discontinuity capacitances in a coaxial low-pass filter would cause an error in cutoff frequency of typically 10–20 percent, and the passband VSWR deteriorates considerably if no compensation for fringing capacitances is made.

In practice, therefore, an exact network synthesis is usually only the first step in the complete design process. Papers on individual components are often written with the main feature distinguishing them from previous contributions being the particular method used to carry out the practical compensations of discontinuity effects. The object of this paper is to introduce design equations and methods common to a large class of distributed reciprocal ladder networks and to demonstrate that certain results in previous papers are special cases of the general formulas.

A possible exception to the above statement, that general techniques have not been available, is the existence of general optimization and search computer techniques, usually referred to as computer-aided design methods. The latter nomenclature is unfortunate if restricted to mean only search algorithms since, as shown in this paper, other types of computer-aided design techniques are available. Search algorithms find limited applications at present, owing to their inability to guarantee either convergence or a true optimum result, and are usually very expensive in terms of computer time. However, these algorithms may be useful in refining the results for networks derived from approximate or imperfect synthesis techniques. (An imperfect synthesis technique is one which does not realize all elements of the physical structure, e.g., fringing capacitances.)

Method

Initially, the design approach is to utilize a suitable prototype network derived by an exact synthesis procedure. The response of the practical component is then forced to fit the response of the ideal prototype as closely as possible. Usually, it will be possible to force exact agreement at only one or two frequencies. Hence it is often desirable to choose a prototype which has a frequency dependence similar to that of the practical distributed component. For this reason, the familiar lumped-element low-pass-filter prototype is often unsuitable, especially for broad-band components. The use of distributed prototypes which are similar to, and occasionally almost identical with, the practical component often results in significantly improved results.

An interesting example of this is the design of inductive-iris direct-coupled cavity filters. The theory based on the lumped-element low-pass prototype [1] breaks down for bandwidths of the order of 10 percent or more. An improved theory for bandwidths as great as 40 percent is based on the quarter-wave-transformer prototype circuit [3], [4], but is not too satisfactory in predicting the skirt attenuation at the larger bandwidths. The basic reason for this is that the frequency dependence of the inductive irises is not taken into account in the quarter-wave-transformer prototype.

The latest theory is based on a distributed prototype which does take this frequency dependence into account, and gives accurate results to bandwidths of at least 100 percent, a bandwidth where the bandpass filter has become in effect a pseudo-high-pass filter [5]. This may not be the end of the story, since research on exact synthesis of mixed lumped and distributed networks may yet produce an exact solution to the problem.

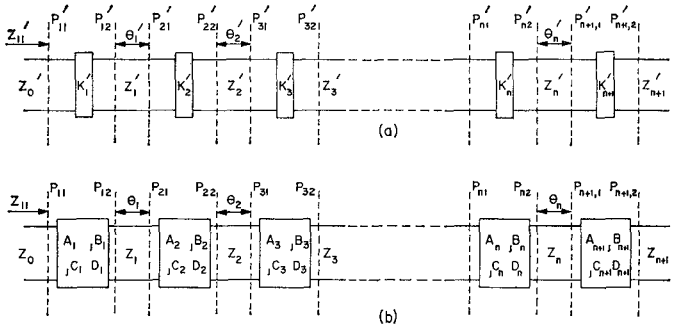

Fig. 1. Distributed ladder networks showing reference planes for (a) the ideal prototype and (b) the physical network.

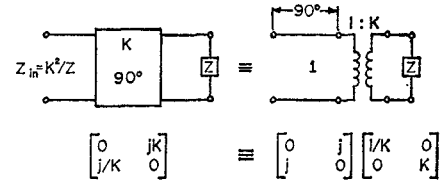

Fig. 2. Definition of an impedance inverter.

Having chosen the most suitable prototype, it is necessary to fit the response of the practical component to it as closely as possible, taking all discontinuity and proximity effects into account. It has been found preferable to compensate for these *ab initio*, rather than attempting the compensation as a separate stage in the design process. These observations do not necessarily apply to components which require fine tuning, such as narrow-band inductive-iris filters. They apply mainly to broad-band components, for example, low-pass filters in the TEM line or waveguide.

The process of matching the practical network of Fig. 1(b) to the prototype of Fig. 1(a) commences by finding characteristic reference planes P_{11}, P_{12}, P_{21}, P_{22}, $\cdots$, which convert each of the lossless passive reciprocal two-ports of the cascade into an ideal impedance inverter at a given reference frequency (for example, the cutoff frequency in the case of a low-pass filter). The normalized characteristic impedance of each inverter and the reference planes are then matched to the corresponding normalized impedance and reference planes of the prototype network. This ensures that the two networks have identical amplitude and phase responses at the reference frequency. The details of this general procedure will now be described.

Generalized Impedance Inverter

The concept of the ideal impedance inverter is well known and is shown in Fig. 2, which is almost self-explanatory. The impedance inverter of impedance K is a *symmetrical* two-port which, looking into its input port, inverts and scales to impedance K any impedance Z connected to its output port. Fig. 2 indicates that the impedance inverter is a cascade of a frequency-independent 90° line and an ideal transformer of turns ratio $1:K$.

A second concept which is not so well known, and has seldom been used, is the means for converting any lossless passive reciprocal two-port into an impedance inverter. The two-port is defined by its transfer matrix

$$\begin{pmatrix} A & jB \\ jC & D \end{pmatrix}$$

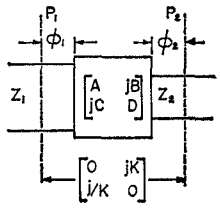

Fig. 3. Location of the characteristic reference planes.

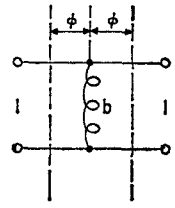

Fig. 4. Shunt-inductance impedance inverter.

and we assume that it is connected to transmission lines of characteristic impedance Z_1 and Z_2 at its two-ports, as shown in Fig. 3. It is a straightforward matter to show that it is always possible to choose reference planes P_1 and P_2 at electrical distances ϕ_1 and ϕ_2 from the respective ports to convert the asymmetric two-port into a symmetric impedance inverter. These reference planes are related to the characteristic reference planes of the Weissfloch equivalent circuit [6], which is an ideal transformer rather than the very similar impedance inverter shown in Fig. 2. The equations giving the reference-plane locations are given in the original in terms of impedance parameters [6], but much simpler and rather symmetrical expressions have been found in terms of the transfer-matrix parameters, leading to the results which follow. Mathematical details of the derivations are given in Appendix I.

Normalization of the transfer-matrix parameters in terms of the terminating line impedances Z_1 and Z_2 gives

$$a = \sqrt{\frac{Z_2}{Z_1}} \qquad b = \frac{B}{\sqrt{Z_1 Z_2}}$$
$$c = C\sqrt{Z_1 Z_2} \qquad d = D\sqrt{\frac{Z_1}{Z_2}}. \tag{1}$$

The characteristic impedance of the inverter K is given by the equation

$$\frac{K}{\sqrt{Z_1 Z_2}} = \sqrt{L} - \sqrt{L-1} = \frac{1}{\sqrt{S}} \tag{2}$$

where L is the insertion loss of the inverter measured between source and load impedances matched, respectively, to Z_1 and Z_2, i.e.,

$$L = 1 + \tfrac{1}{4}(a-d)^2 + \tfrac{1}{4}(b-c)^2. \tag{3}$$

The normalized characteristic impedance of the inverter is $K/\sqrt{Z_1 Z_2}$, which is the quantity to be made invariant when matching a practical network to a prototype. S is the VSWR seen at one port of the inverter when the other port is terminated in its characteristic impedance. The reference-plane locations are given by the equations

$$\tan 2\phi_1 = \frac{2(bd-ac)}{(a^2-d^2)+(b^2-c^2)}$$
$$\tan 2\phi_2 = \frac{2(ab-cd)}{(d^2-a^2)+(b^2-c^2)}. \tag{4}$$

Note from (4) that an infinite number of characteristic reference planes exist, half of which correspond to the Weissfloch equivalent and half to the impedance-inverter equivalent. In practice, planes closest to the two-port are chosen. ϕ_1 or ϕ_2 may be realized as negative values in practice by absorbing such a negative value into the adjacent positive line length, which therefore becomes shortened in the final network.

Application of the Generalized Impedance Inverter

We are now in a position to comprehend the method of equating the prototype of Fig. 1(a) to the physical realization of Fig. 1(b). The normalized inverter impedance and characteristic reference planes of each element of the prototype are determined, using (1)–(4). The corresponding quantities are found for the practical network of Fig. 1(b), taking all fringing and practical junction effects into account as far as possible. The dimensions of the practical device are chosen to give exact equivalence between the normalized inverter impedances of the prototype and of the physical network at a reference frequency. This process usually requires an iteration technique implemented by means of a computer program. The electrical lengths between the reference planes of the prototype and practical networks are then forced to coincide, i.e.,

$$\theta_i = \theta_i', \qquad i = 1, 2, \cdots, n. \tag{5}$$

The prototype and practical networks now have identical amplitude response (except for a possible impedance scaling factor) at the reference frequency, and also identical phase if the networks are delineated by the outer reference planes P_{11}', $P_{n+1,2}'$ and P_{11}, $P_{n+1,2}$.

Note that it is not necessary for the impedances of the connecting transmission lines of the prototype and practical networks to be equal, and the two networks can differ only by an overall scaling factor on the impedance level. The proof of this statement is given in Appendix II. However, in many cases it will be convenient to choose the corresponding impedances to be equal, especially since any deviation from the prototype values may cause the broad-band performance of the component to deteriorate. The object is to choose a prototype which closely approximates the *broad-band characteristics* of the practical component; if differences in the impedances of the connecting lines are desired, it is usually preferable to change the prototype rather than to utilize the flexibility of the choice of impedances in the component. An example of the change in performance caused by changing the impedance levels is given in [5, figs. 8 and 9]. In that case, the impedances of the connecting lines were changed by factors of between unity and 2.5, and the broad-band performance suffered a considerable (but often acceptable) deterioration.

Special Cases of the Generalized Impedance Inverter

Example 1—Shunt Inductance

It is interesting to see how (1)–(4) simplify to give the well-known results for the simple inverter used in inductive-iris filters. This consists of a shunt susceptance b at the center of a unit impedance line of electrical length 2ϕ, as shown in Fig. 4.

The transfer matrix of the susceptance is

$$\begin{pmatrix} 1 & 0 \\ jb & 1 \end{pmatrix} \tag{6}$$

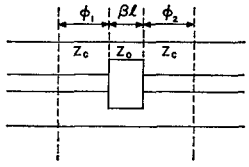

Fig. 5. Coaxial disk capacitor. $\phi_1=\phi_2=\phi/2$.

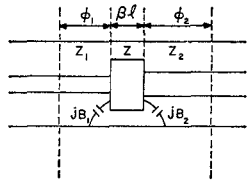

Fig. 6. General coaxial disk capacitor with fringing capacitances.

and the insertion loss is

$$L = 1 + b^2/4. \tag{7}$$

Hence the inverter impedance is given from (2) as

$$K = \sqrt{1 + b^2/4} - b/2 \tag{8}$$

leading to the well-known expression [1]

$$b = 1/K - K. \tag{9}$$

Substituting $a=d=1$, $c=0$, and $b=b$ in (4) gives

$$\tan 2\phi = 2/b \tag{10}$$

as required.

Example 2—Coaxial Disk Capacitor

An impedance inverter consisting of a length of low-impedance ($=Z_0$) transmission line with high-impedance ($=Z_c$) lines on either side as shown in Fig. 5 was treated by Davis and Khan [7]. Their derivation of the impedance-inverter parameters simplifies considerably when the general design equations (1)–(4) are applied to the transfer matrix:

$$\begin{pmatrix} \cos\beta l & jZ_0 \sin\beta l \\ \dfrac{j}{Z_0}\sin\beta l & \cos\beta l \end{pmatrix} \tag{11}$$

Noting that $Z_1=Z_2=Z_c$, (2) becomes

$$\frac{Z_c}{K} - \frac{K}{Z_c} = 2\sqrt{L-1} = \left(\frac{Z_0}{Z_c} - \frac{Z_c}{Z_0}\right)\sin\beta l. \tag{12}$$

Using the definition of a quantity E, [7, eq. (13)] leads to

$$E = \left[\frac{\dfrac{K}{Z_c}}{1-\left(\dfrac{K}{Z_c}\right)^2}\right]\left[\frac{\dfrac{Z_0}{Z_c}}{1-\left(\dfrac{Z_0}{Z_c}\right)^2}\right]^{-1} = \sin\beta l \tag{13}$$

in agreement with [7, eq. (14)], which is used there to determine the magnitude of the impedance inverter.

In the case when $a=d$, (4) simplifies to give

$$\tan 2\phi_1 = \tan 2\phi_2 = \frac{2a}{b+c} = \tan\phi. \tag{14}$$

In the case under consideration, we have

$$a = \cos\beta l, \quad b = \frac{Z_0}{Z_c}\sin\beta l, \quad c = \frac{Z_c}{Z_0}\sin\beta l \tag{15}$$

so that (14) becomes

$$\tan\phi = \frac{2\cos\beta l}{\left(\dfrac{Z_0}{Z_c}+\dfrac{Z_c}{Z_0}\right)\sin\beta l}$$

or

$$\tan\beta l \tan\phi = \frac{2}{\dfrac{Z_0}{Z_c}+\dfrac{Z_c}{Z_0}} \tag{16}$$

which is identical to [7, eq. (7)].

Example 3—Disk Capacitor with Fringing Effects

The previous examples, while trivial, illustrate the mathematical simplifications to be gained over previous techniques, but the complete power of the general equations is not evident unless a more complex asymmetric case with fringing effects is illustrated. The simple symmetric capacitive disk impedance inverter treated in Example 2 was used in [7] to design half-wave coaxial bandbass filters. In [7], the fringing capacitances were compensated by one of three different methods after the filter had been designed, assuming no fringing effects. This approach is subject to varying success as described in [7]. The most successful of the compensation techniques, introduced in a previous paper of the author [8] and denoted in [7] as method 3, does not always converge. However, this method should now be considered technically obsolete, being replaced by the general design equations (1)–(4) of this paper, as applied to the particular situation illustrated in Fig. 6.

The transfer matrix of the basic two-port network is

$$\begin{pmatrix} A & B \\ C & D \end{pmatrix} = \begin{pmatrix} 1 & 0 \\ jB_1 & 1 \end{pmatrix}\begin{pmatrix} \cos\beta l & j\sin\beta l \\ \dfrac{j\sin\beta l}{Z} & \cos\beta l \end{pmatrix}\begin{pmatrix} 1 & 0 \\ jB_2 & 1 \end{pmatrix}$$

$$= \begin{pmatrix} \cos\beta l - B_2 Z\sin\beta l & jZ\sin\beta l \\ j\left[(B_1+B_2)\cos\beta l + \left(\dfrac{1}{Z} - B_1B_2Z\right)\sin\beta l\right] & \cos\beta l - B_1 Z\sin\beta l \end{pmatrix}. \tag{17}$$

The inverter impedance may now be written down by application of (2). If, as is usually the case, a given inverter impedance is desired and the length l is required, a simple iteration technique may be used. Unlike the method used in [8], this technique always converges, except in extreme cases where the fringing capacitances alone are themselves so

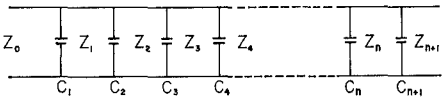

Fig. 7. Low-pass prototype filter.

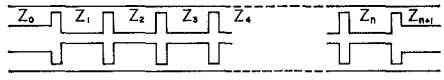

Fig. 8. Coaxial low-pass filter.

large that a negative value of βl results. It is then possible to decrease the magnitude of the junction discontinuities to ensure convergence merely by increasing Z.

The locations of the reference planes are found by application of (4) to the transfer-matrix parameters, and complete compensation for the fringing capacitances will have been accomplished.

Practical Ladder-Network Synthesis

A number of methods are available for carrying out the complete process of practical ladder-network synthesis by means of a digital-computer program. The discontinuity, junction, and proximity effects are stored either as closed-form expressions or as numerical data subject to interpolation. The prototype network is synthesized to fit the specification, either within the practical design program or the prototype parameters are fed in as data. The prototype and practical networks are divided into a cascade of impedance inverters and the program causes these to be identical at the reference frequency. This requires an iteration technique programmed to be rapidly convergent. The result is printed out as a set of dimensions for the actual component, which may then be computer analyzed over the required band to check its performance. This will be slightly inferior to that of the prototype, except at the reference frequency where the performance should be as predicted, providing one check on the accuracy of the program. A second check is given by measurement of the actual manufactured component, which should give results in almost perfect agreement with the computer analysis if the electromagnetic data stored within the computer are accurate.

Example—Coaxial Low-Pass Filters

Assume that the prototype network consists of a cascade of ideal shunt capacitances alternating with equal length transmission lines, as shown in Fig. 7. This may be synthesized by the method given in [5]. This network is to be realized practically as a coaxial structure whose cross section is shown in Fig. 8. Here, the ideal shunt capacitances are replaced by short lengths of low-impedance lines, and hence are no longer purely capacitive. Since the spacings between these disks are much less than one wavelength in the low-pass band, then mutual interactions between adjacent disks must be taken into account.

A flow diagram of the computer program is given in Fig. 9. The inverter impedance and characteristic reference planes of each element of the prototype (in this case, each shunt capacitor) are determined. The diameters of the capacitive disks in Fig. 8 are then chosen at some fixed value, which (apart from the proximity effect) also fixes the value of the fringing capacitances, given by a formula described later. A rather close initial value of the thickness of a given disk may

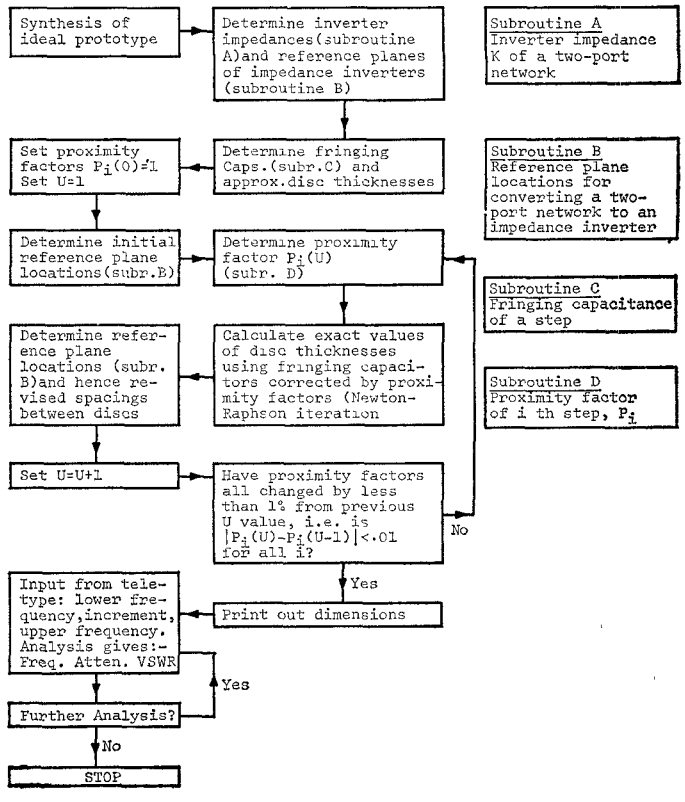

Fig. 9. Program flow chart.

now be given if we assume initially that it is a simple cylindrical capacitor plus the fringing capacitors. The exact inverter-impedance parameters are given in Example 3. Later in the program we will force the inverter impedance of the exact two-port circuit to be equal to that of the prototype and will determine the characteristic reference planes of each disk. The distances between reference planes of the prototype and physical circuits are made equal at the chosen cutoff frequency, which consequently determines the spacing of the disks.

This would complete the design if it were not for the possible existence of finite proximity effects, given for any pair of adjacent disks as a factor P_i by which each fringing capacitor should be multiplied. The calculation of P_i in a subroutine is described later. The means by which the proximity factors P_i are taken into account are indicated in the flow chart (Fig. 9). Initially, the proximity factors are set equal to unity and are stored as an array under a second variable U initially set equal to zero. After the initial values of reference-plane locations have been determined, an initial estimate of the proximity factors may be made and stored under $U=1$. These are used to correct the fringing-capacitance values. The corresponding exact values of the disk thicknesses may be found by iteration and then the corrected reference-plane locations. At this stage we say that if all the proximity factors are within 1 percent of their previously estimated values stored under $U=0$, we jump out of the loop and print out the final set of dimensions. Otherwise, we determine a new set of proximity factors and continue in the loop. Since P_i is rarely less than 0.8, the process converges rapidly.

The final part of the program is to analyze the complete circuit using multiplication of transfer matrices, the exact values of the fringing capacities being determined at each

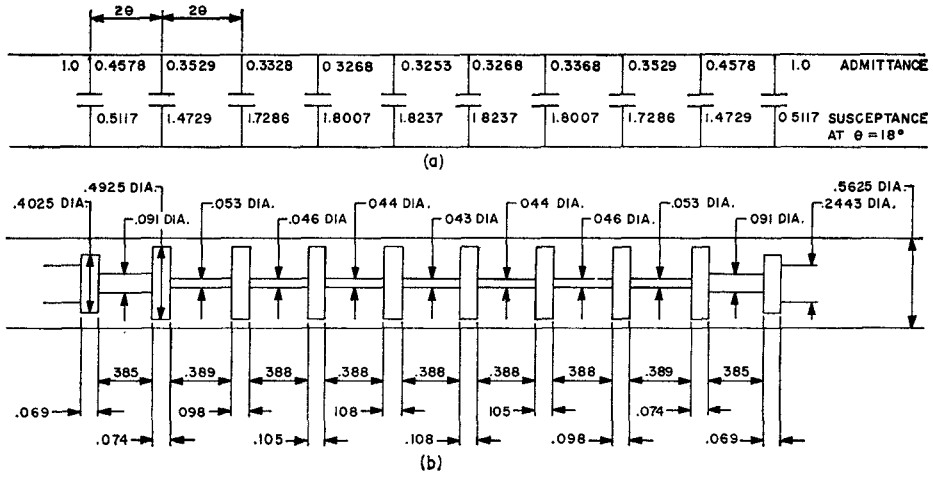

Fig. 10. (a) Mixed lumped and distributed prototype. (b) Coaxial realization (dimensions in inches).

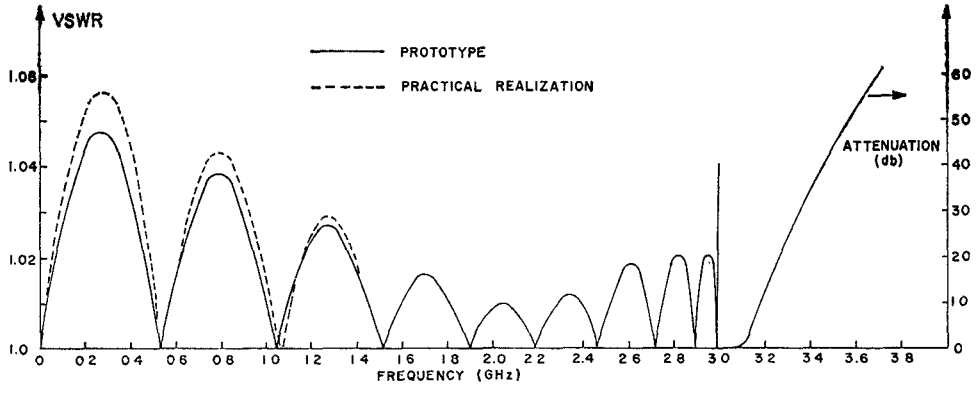

Fig. 11. Computed VSWR and attenuation of prototype filter shown in Fig. 10(a) and practical realization of Fig. 10(b).

frequency using subroutine C. As stated previously, this is an essential part of any synthesis program, giving both a useful check on the validity of the synthesis and the actual response of the component.

Subroutines A and B have been described previously, A being given by (1)–(3) and B by (4).

The fringing capacitance is determined in subroutine C using the simple formula given by Somlo [9, p. 49]. This is modified by multiplication by the frequency-correction factor K (not to be confused with an inverter impedance) discussed by Somlo, and plotted in [9, fig. 3]. However, since K is only slightly greater than unity, it is sufficiently accurate to use the formula

$$K = \left(1 - \left(\frac{2b}{\lambda}\right)^2\right)^{-1/2} \tag{18}$$

where b and λ are defined in [9].

If dielectric supports for the capacitive disks are used, the fringing capacitances are assumed to be unaffected, since the fringing fields are mainly in the air regions.

The proximity effect subroutine D consists of a set of specific values given by Green [10, fig. 9]. Interpolation between successive curves denoted by parameter β is carried out using the fact that P is given approximately by $\tanh(\pi\beta)$. Interpolation between successive values of the variable α is taken as linear.

These subroutines and all other steps in the program are very rapid. For example, a complete design on a time-shared terminal using a CDC 3600 for a high-ordered filter uses approximately 8 s of CPU time and a few minutes of connect time.

Example designs for low-pass-filter prototypes are given in [5] and a practical example for an impedance-transforming filter in [11]. Now it is interesting to redesign a low-pass filter for the specification given in [8, fig. 6], giving a direct comparison between the previous method and that described here. A suitable prototype derived by the method given in [5] is shown in Fig. 10(a) and the dimensions of the filter in Fig. 10(b). A comparison between the computed performances of the prototype and practical filters is given in Fig. 11, and indicates negligible difference. The filter was chosen to give the same in-band VSWR and rate of cutoff as the filter given in [8, figs. 5 and 6], but is only 4.396 in in length compared with 11.467 in previously.

The coaxial low-pass filter is a rather favorable example, but equally good results have been obtained for rectangular-waveguide low-pass filters using capacitive irises [12] and stripline high-pass filters using series capacitive gap coupling (taking all fringing effects into account).

Appendix I

Derivation of the General Impedance-Inverter Equations

The transfer matrix of the two-port network defined between reference planes P_1 and P_2 in Fig. 3 is

$$\begin{pmatrix} A' & jB' \\ jC' & D' \end{pmatrix} = \begin{pmatrix} \cos\phi_1 & jZ_1 \sin\phi_1 \\ \dfrac{j\sin\phi_1}{Z_1} & \cos\phi_1 \end{pmatrix} \begin{pmatrix} A & jB \\ jC & D \end{pmatrix} \cdot \begin{pmatrix} \cos\phi_2 & jZ_2 \sin\phi_2 \\ \dfrac{j\sin\phi_2}{Z_2} & \cos\phi_2 \end{pmatrix} \quad (19)$$

which, by definition, is an impedance inverter if $A' = D' = 0$, i.e., if

$$\left(A\cos\phi_2 - \frac{B}{Z_2}\sin\phi_2\right)\cos\phi_1 - Z_1\sin\phi_1 \cdot \left(C\cos\phi_2 + \frac{D}{Z_2}\sin\phi_2\right) = 0 \quad (20)$$

$$\left(D\cos\phi_2 - CZ_2\sin\phi_2\right)\cos\phi_1 - \frac{\sin\phi_2}{Z_1} \cdot \left(B\cos\phi_2 + AZ_2\sin\phi_2\right) = 0. \quad (21)$$

Defining

$$\tan\phi_1 = t_1 \qquad \tan\phi_2 = t_2 \quad (22)$$

and dividing (20) and (21) by $\cos\phi_1 \cos\phi_2$ gives

$$A - \frac{B}{Z_1}t_2 - CZ_1t_1 - \frac{DZ_1}{Z_2}t_1t_2 = 0 \quad (23)$$

$$D - CZ_2t_2 - \frac{B}{Z_1}t_1 - A\frac{Z_2}{Z_1}t_1t_2 = 0. \quad (24)$$

Solving (23) for t_2 and substituting in (24) gives

$$\left(D - \frac{B}{Z_1}t_1\right) - \left(CZ_2 + A\frac{Z_2}{Z_1}t_1\right)\frac{(A - CZ_1t_1)Z_2}{(B + DZ_1t_1)} = 0$$

or

$$\left(\frac{BD}{Z_2} - ACZ_2\right)(1 - t_1^2) + \left(\frac{D^2Z_1}{Z_2} - \frac{B^2}{Z_1Z_2} + C^2Z_1Z_2 - \frac{A^2Z_2}{Z_1}\right)t_1 = 0. \quad (25)$$

Using the identity

$$\tan 2\phi = \frac{2\tan\phi}{1 - \tan^2\phi} \quad (26)$$

then (25) can be rearranged to give

$$\tan 2\phi_1 = \frac{2\left(\dfrac{BD}{Z_2} - ACZ_2\right)}{A^2\dfrac{Z_2}{Z_1} + \dfrac{B^2}{Z_1Z_2} - C^2Z_1Z_2 - D^2\dfrac{Z_1}{Z_2}}. \quad (27)$$

Using the normalization given in (1), then (27) is recognized as the first of (4). The second such equation is derived by interchanging A and D and subscripts 1 and 2 in (27).

Equation (2) is derived by noting that the insertion loss of the impedance inverter is given by

$$L = 1 + \frac{1}{4}\left(\frac{K}{\sqrt{Z_1Z_2}} - \frac{\sqrt{Z_1Z_2}}{K}\right)^2 \quad (28)$$

which may be solved to give K as a function of L, resulting in (2) Note that K is independent of the location of reference planes P_1 and P_2.

Appendix II

Variation of Internal Impedance Levels

Assume that the prototype network shown in Fig. 1(a) is terminated in resistances matched to the line impedance at either end. Then the impedance looking to the right at reference plane P_{n2}' is

$$Z_{n2}' = Z_n' \frac{\dfrac{K_{n+1}'}{Z_n'Z_{n+1}'} + j\tan\theta_n'}{1 + j\dfrac{K_{n+1}'^2}{Z_n'Z_{n+1}'}\tan\theta_n'}. \quad (29)$$

The impedance at reference plane P_{n2} in the practical component shown in Fig. 1(b) is given by an expression identical to (29), except that the primes are suppressed. Hence we see that

$$\frac{Z_{n2}}{Z_n} = \frac{Z_{n2}'}{Z_n'} = C_n \quad (30)$$

if

$$\theta_n = \theta_n' \quad (31)$$

and

$$\frac{K_{n+1}^2}{Z_nZ_{n+1}} = \frac{K_{n+1}'^2}{Z_n'Z_{n+1}'}. \quad (32)$$

Similarly, the impedance at reference plane $P_{n-1,2}'$ normalized to Z_{n-1}' is

$$\frac{Z_{n-1,2}'}{Z_{n-1}'} = \frac{\dfrac{K_n'^2}{Z_{n-1}'Z_{n2}'} + j\tan\theta_{n-1}'}{1 + j\dfrac{K_n'^2}{Z_{n-1}'Z_{n2}'}\tan\theta_{n-1}'} \quad (33)$$

which again is invariant if θ_{n-1}' and $K_n'^2/Z_{n-1}'Z_n'$ are invariant, since by (30), Z_{n2}' and Z_n' are related through a constant C_n.

Finally, transferring the impedance through the entire network gives a final relationship

$$\frac{Z_n}{Z_0} = \frac{Z_n'}{Z_0'} \tag{34}$$

showing that the networks are identical apart from an overall scaling factor.

References

[1] S. B. Cohn, "Direct-coupled-resonator filters," *Proc. IRE*, vol. 45, pp. 187–196, Feb. 1957.

[2] L. Young, "The quarter-wave transformer prototype circuit," *IRE Trans. Microwave Theory Tech.*, vol. MTT-8, pp. 483–489, Sept. 1960.

[3] ——, "Direct-coupled cavity filters for wide and narrow bandwidths," *IEEE Trans. Microwave Theory Tech.*, vol. MTT-11, pp. 162–178, May 1963.

[4] R. Levy, "Theory of direct-coupled-cavity filters," *IEEE Trans. Microwave Theory Tech.*, vol. MTT-15, pp. 340–348, June 1967.

[5] ——, "A new class of distributed prototype filters with applications to mixed lumped/distributed component design," *IEEE Trans. Microwave Theory Tech.* (*1970 Symposium Issue*), vol. MTT-18, pp. 1064–1071, Dec. 1970.

[6] N. Marcuvitz, Ed., *Waveguide Handbook* (M.I.T. Radiation Laboratory Series), vol. 8. New York: McGraw-Hill, 1951, pp. 120–124.

[7] W. A. Davis and P. J. Khan, "Coaxial bandpass filter design," *IEEE Trans. Microwave Theory Tech.*, vol. MTT-19, pp. 373–380, Apr. 1971.

[8] R. Levy and T. E. Rozzi, "Precise design of coaxial low-pass filters," *IEEE Trans. Microwave Theory Tech.*, vol. MTT-16, pp. 142–147, Mar. 1968.

[9] P. I. Somlo, "The computation of coaxial line step capacitances," *IEEE Trans. Microwave Theory Tech.*, vol. MTT-15, pp. 48–53, Jan. 1967.

[10] H. E. Green, "The numerical solution of some important transmission-line problems," *IEEE Trans. Microwave Theory Tech.*, vol. MTT-13, pp. 676–692, Sept. 1965.

[11] R. Levy, "Synthesis of mixed lumped and distributed impedance-transforming filters," *IEEE Trans. Microwave Theory Tech.*, vol. MTT-20, pp. 223–233, Mar. 1972.

[12] ——, "Tapered corrugated waveguide low-pass filters," this issue, pp. 526–532.

Tapered Corrugated Waveguide Low-Pass Filters

RALPH LEVY

Abstract—**Several new synthesis techniques are described for the design of tapered corrugated waveguide low-pass filters. Previous techniques are based on image-parameter methods which are both nonoptimum and difficult to apply to new specifications. The new synthesis methods give filters which can be constructed to work directly from dimensions generated by a computer. The impedance tapering implies that the terminating impedance transformers used in the image-parameter designs may be either eliminated or reduced in length.**

Introduction

WAVEGUIDE low-pass filters are used in numerous systems, frequently for rejection of spurious harmonics from transmitters. Corrugated waveguide or waffle-iron filters introduced by Cohn [1] are most commonly used for this purpose. The first design methods described in the literature [2] are based on image parameters rather than modern circuit theory, and involve rather complicated procedures requiring empirical adjustments to experimental filters before a satisfactory final design is achieved. Later methods using synthesis techniques have been described very briefly [3] and appear as patents [4], [5]. This paper gives a more complete account of synthesis techniques, including some not reported in the earlier publications.

The major advantages of the synthesis techniques are as follows.

1) The filters may be constructed directly from dimensions printed out by a computer program and work immediately with no major experimental adjustments. In common with other types of waveguide filters, minor tuning adjustments may be required to compensate for mechanical tolerances, especially in small waveguide sizes.

2) The synthesis technique incorporates impedance tapering, so that terminating impedance transformers required in previous designs [2] may be shorter in length, or even completely eliminated. This can result in a length reduction by as much as 3 to 1.

3) The cutoff frequency is predicted exactly, and the VSWR is good in a specified frequency band extending to the cutoff. Hence high attenuation may be specified close to the cutoff frequency f_c, typically 20 dB at $1.05f_c$, or 60 dB at $1.15f_c$.

4) The stopband performance is predicted.

5) Tradeoffs may be made between stop bandwidth, passband insertion loss, and power handling capability.

Several different synthesis techniques have been formulated, but they may be classified in three main categories, as follows.

1) Tapered corrugated capacitive iris filters designed using the distributed low-pass prototype filter [6].

2) Direct realization of a tapered corrugated filter designed using a cascade of unit elements similar to [6], but with a Zolotarev response.

3) A mixed lumped and distributed synthesis using the "half-stub" prototype [7].

The first two methods have been found more generally useful than the third. They are more dissimilar than indicated above, as the detailed description will demonstrate.

A schematic view of the tapered corrugated filter is shown in Fig. 1. The early corrugated filters were periodic structures, but the new designs result in aperiodic structures where the dimensions of the various capacitive and inductive regions

Manuscript received December 6, 1972; revised March 23, 1973.

The author is with Microwave Development Laboratories, Inc., Natick, Mass. 01760.